Periodica Polytechnica
Civil Engineering

59(4), pp. 511–520, 2015
DOI: 10.3311/PPci.8410

RESEARCH ARTICLE

The Influence of Lintel Beams and Floor Slabs on Natural Frequencies of the Tall Buildings Core - Numerical and Experimental Studies

György Varjú, *Aleksandar* Prokić
Received 15-07-2015, accepted 07-09-2015

Abstract

This paper presents the analysis of influence of lintel beams and floor slabs on natural frequencies of tall buildings, braced by core walls. For that purpose a numerical procedure based on the Vlasov theory of thin-walled beams and transfer matrix method has been developed. In order to check the accuracy of the proposed method the calculated results are compared with those obtained by FEM and experiment. Based on these results the effects of the lintel beams and floor slabs on the natural frequencies of the tall buildings core are discussed

Keywords

thin-walled beam · core of tall buildings · transfer matrix method · coupled vibration analysis · experimental test

György Varjú

Department of Engineering Mechanics, Faculty of Civil Engineering Subotica, University of Novi Sad, 24000 Subotica, Serbia
e-mail: varjugy@gf.uns.ac.rs

Aleksandar Prokić

Department of Engineering Mechanics, Faculty of Civil Engineering Subotica, University of Novi Sad, 24000 Subotica, Serbia
e-mail: aprokic@eunet.rs

1 Introduction

In the case of tall buildings, the influence of transverse loading caused by winds or seismic activity can be significant. This load is most often supported by a reinforced concrete core, which houses the elevator shaft or the staircase of the building. Due to the small thickness of the core walls compared to the dimensions of the cross section, which, again, are small compared to the height of the building, according to the Vlasov theory, the core can be treated as a thin-walled, open cross section cantilever beam. Floors act as transverse stiffeners providing the necessary cross section rigidity of the core. The core foundation is usually stiff enough, so full restraint can be assumed.

If the shear centre of the core cross section is located asymmetrically in respect to the base of the building, or if the transverse loading is eccentric, the core is, apart from bending, exposed to torsion, as well. In the case of taller buildings the torsion influences are greater, so it is necessary to provide appropriate torsional rigidity to the core. Lintel beams connecting the core walls at each floor level, as well as floor slabs, also contribute to torsional rigidity. The influence of these elements on the total torsional rigidity of the core can be significant, as will be highlighted in the examples given below.

Papers by Liauw and Luk [1] and Mendis [2] investigate static behaviour of core of tall buildings, taking into account the influence of lintel beams. In their static analysis of the core, Smith and Taranath [3] and Heidebrecht and Smith [4] consider the influence of floor slabs as well as the influence of lintel beams on torsional rigidity of the core. The analysis of dynamic behaviour of the core in tall buildings was given in the papers by Ng and Kuang [5], Kuang and Ng [6], Mehtaf and Tounsi [7], Rafezy and Howson [8] and Kheyroddin, Abdollahzadeh and Mastali [9]. These works, though, did not specifically discuss the influence of floor slabs and lintel beams on the dynamic behaviour of buildings. Zalka, [10] and [11], considered the joined influence of bracing elements (frameworks, shear walls and core as well) in the case of a multi-storey building subjected to horizontal load. His model treats floor slabs stiff in their plane connected by stiff pinned bars to their surroundings, i.e. the out-of-plane stiffness is assumed zero. Kollár [12] analysed natural frequency

(NF) of thin-walled open section composite beams according to the Vlasov theory modified to include transverse shear and restrained warping induced shear deformations. Pluzsik and Kollár [13] developed a simple expression to determine the effect of shear deformation in thin-walled beams. Potzta and Kollár [14] developed a method for building analysis applying replacement sandwich beams, accounting for shear deformation, as well. Zalka [15] proposed a closed -form solution for the analysis of deflection in tall buildings (braced by frames, shear walls and cores), substituted by an equivalent column. In this study, besides bending deformation, shear deformation is accounted for.

The purpose of this article is to investigate the change in the magnitude of NFs of tall buildings braced by core only, caused by the action of lintel beams and floor slabs. For that, a relatively simple numerical method, based on the Vlasov theory of thin-walled beams and transfer matrix method, has been developed.

The core was longitudinally divided, floor to floor, in segments. Mass distribution was idealized by concentrating masses of each segment at the corresponding floor slab level, in the common centre of masses. Computer program TWBEIG written in Visual Fortran was developed for the presented procedure to calculate NFs. In order to verify the proposed method, the results presented in this paper were compared to FEM results and with results of an experimental test carried out on a plexiglass model.

2 Analytical model

The thin-walled beam is analysed in the Cartesian coordinate system *OXYZ*, whose $Z-$axis connects the centroids O of the cross sections, and axes X and Y were chosen to match the main central axes of inertia of the cross section. Starting from usual assumptions of the Vlasov theory:

- the cross-section is perfectly rigid in its own plane,
- the shear strains in the middle surface of the wall are negligible.
- There is no shear strain in the plane perpendicular to the middle surface (Kirchhoff's thin plate bending assumption),

the governing equations of motion of the thin-walled beam can be formulated as three coupled differential equations [16]:

$$\begin{aligned} &EI_{XX}u'''' - \rho I_{XX}\ddot{u}'' + \rho F\ddot{u} + \rho FY_D\ddot{\varphi} = p_X - m_Y', \\ &EI_{YY}v'''' - \rho I_{YY}\ddot{v}'' + \rho F\ddot{v} - \rho FX_D\ddot{\varphi} = p_Y - m_X', \\ &EI_{\Omega\Omega}\varphi'''' - GK\varphi'' - \rho I_{\Omega\Omega}\ddot{\varphi}'' + \rho FY_D\ddot{u} - \\ &- \rho FX_D\ddot{v} + \rho I_D\ddot{\varphi} = m_D + m_\Omega, \end{aligned} \tag{1}$$

where the basic unknowns $u = u_D(Z,t)$, $v = v_D(Z,t)$ and $\varphi = \varphi_D(Z,t)$ are the displacement of shear centre D in the X and Y direction, and the rotation of cross section around the shear axis, E = modulus of elasticity, G = shear modulus, F = cross-sectional area, and ρ = mass density of the thin-walled beam. p_X, p_Y, m_X, m_Y, m_D and m_Ω represent external distributed loads per unit length in the X - and Y - directions, externally applied distributed moments per unit length around the X, Y and the shear axes, and external distributed warping moment (bimoment) respectively. X_D and Y_D are the coordinates of point D, and I_{XX} and I_{YY} are the moments of inertia in relation to principal axes, $I_{\Omega\Omega}$ is sectorial moment of inertia, K is the Saint Venant's torsional constant and I_D is the mass moment of inertia in respect to the same point.

The free harmonic vibrations are defined by the coupled homogeneous equations (1). The solution may be expressed as:

$$\begin{aligned} u(Z,t) &= U(Z)\,sin(\omega t), \\ v(Z,t) &= V(Z)\,sin(\omega t), \\ \varphi(Z,t) &= \Phi(Z)\,sin(\omega t). \end{aligned} \tag{2}$$

$U(Z)$, $V(Z)$ and $\Phi(Z)$ are amplitudes of the basic unknown variables, which depend on the Z coordinate only and ω is the circular frequency. Substituting expressions (2) in equations (1) yields:

$$\begin{aligned} &EI_{XX}U'''' + \rho\omega^2 I_{XX}U'' - \rho F\omega^2(U + Y_D\Phi) = 0, \\ &EI_{YY}V'''' + \rho\omega^2 I_{YY}V'' - \rho F\omega^2(V - X_D\Phi) = 0, \\ &EI_{\Omega\Omega}\Phi'''' - GK\Phi'' + \rho\omega^2 I_{\Omega\Omega}\Phi'' - \\ &- \rho F\omega^2(Y_DU - X_DV + I_D\Phi) = 0. \end{aligned} \tag{3}$$

Knowing the state vector at the lower endpoint of each segment, the state vector at the upper endpoint can be determined by the transfer-matrix method, using solution of differential equations (3). The state vector $\{S\}$ of the basic unknowns

$$\begin{aligned} \{S\} = \Big\{ &U, U', \frac{M_Y}{EI_{XX}}, \frac{Q_X}{EI_{XX}}, \\ &V, -V', \frac{M_X}{EI_{YY}}, \frac{Q_Y}{EI_{YY}}, \Phi, \Phi', \frac{B}{GK}, \frac{T}{GK} \Big\}^T \end{aligned} \tag{4}$$

comprises of generalized displacements, its derivatives and generalized forces

$M_Y = M_Y(Z,t) = EI_{XX}U''$ bending moment around the Y axis,
$Q_X = Q_X(Z,t) = -EI_{XX}U'''$ shear force in the X direction,
$M_X = M_X(Z,t) = -EI_{YY}V''$ bending moment around the X axis,
$Q_Y = Q_Y(Z,t) = -EI_{YY}V'''$ shear force in the Y direction,
$B = B(Z,t) = -EI_{\Omega\Omega}\Phi''$ bimoment,
$T = T(Z,t) = GK\Phi' - EI_{\Omega\Omega}\Phi'''$ torsion moment around the shear axis.

2.1 Transfer-matrix method

In longitudinal direction the core of the building consists of n segments and floors. The marking (numbering) of floors starts at the foundation and rises towards the top. The segment marked m is between the floors marked $m-1$ (lower level) and m (higher

level). The generalized forces at the endpoints of the segment are shown in Fig. 1.

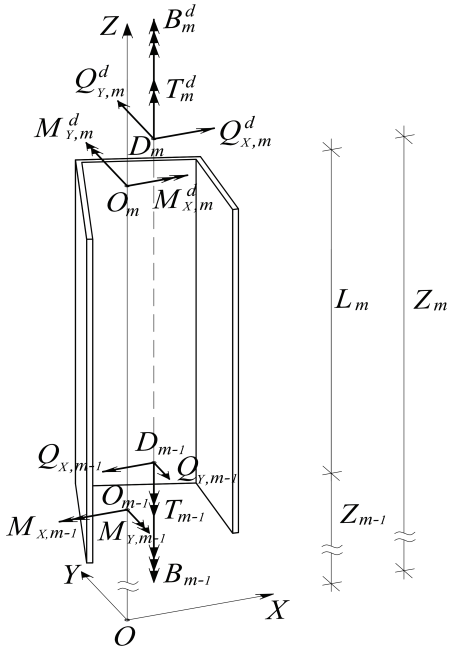

Fig. 1. Generalized forces at the endpoints of segment *m*

Longitudinally the wall thickness of the cross section is constant within the observed segment, but it can change from segment to segment. At the same time, centroids and the shear centre of cross sections always remain on the same axes. The geometrical characteristics of core cross section refer only to a specific segment.

The beam and the slab are made of same material as the core, therefore the physical characteristics, such as E, G and ρ are the same as for the core. The forces due to lintel beams and floor slabs, as well as inertia forces that act in the center of masses C, are reduced to the nodes.

Taking in account that the total mass of the model is concentrated in the center of masses corresponding to each level (inertial forces act only at the endpoints of each segment), equations (3) related to a particular segment are given as follows:

$$\begin{aligned} EI_{XX}U'''' &= 0, \\ EI_{YY}V'''' &= 0, \\ EI_{\Omega\Omega}\Phi'''' - GK\Phi'' &= 0. \end{aligned} \tag{5}$$

The solution of the differential equations (5) is obtained in a matrix form as following:

$$\left\{S_m^d\right\} = [A_{m,s}]\,\{S_{m-1}\}, \tag{6}$$

where $\left\{S_m^d\right\}$ and $\{S_{m-1}\}$ are the state vectors below node m and above node m-1, respectively, and $[A_{m,s}]$ is the transfer matrix of segment m, see Appendix.

In each node of the core the generalized forces act infinitely closely above and below the node, and in the node itself. The generalized forces acting just above node m are denoted by a lower index m. The forces acting in the node itself represent bimoments (due to the corresponding lintel beam and floor slab) and inertia forces. They are denoted by subscript m and upper line. The generalized forces in the cross section just below node m are denoted by subscript m and superscript d (see Fig. 2).

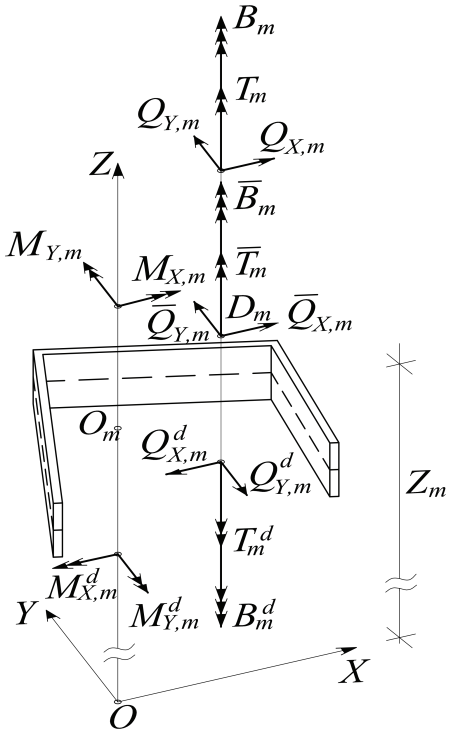

Fig. 2. Generalized forces in node *m*

When the construction is subject to vibration, masses are exposed to acceleration, inducing inertia forces and inertia torque in respect to the center of mass C. Reduced to node D, they are:

$$\begin{aligned} \bar{Q}_X &= \omega^2\,(M\,U + M\,Y_{DC}\,\Phi), \\ \bar{Q}_Y &= \omega^2\,(M\,V - M\,X_{DC}\,\Phi), \\ \bar{T} &= \omega^2\,(M\,Y_{DC}\,U - M\,X_{DC}\,V + J_D\,\Phi), \end{aligned} \tag{7}$$

where M is the mass reduced to center C, Y_{DC} and X_{DC} are projections of distance between points C and D on the Y and X axes, respectively.

The transfer matrix of node m is obtained by exploiting compatibility and equilibrium conditions in the node, considering forces acting just above and below the node, and in the node itself. The relation between the state vectors above and below the node is:

$$\{S_m\} = [A_{m,n}]\left\{S_m^d\right\}, \tag{8}$$

where $[A_{m,n}]$ is the transfer matrix of node m, see Appendix.

The connection between the state vectors of node $m-1$ and node m is obtained by substituting the matrix relation (6) into (8):

$$\begin{aligned} \{S_m\} &= [A_{m,n}]\left\{S_m^d\right\} = \\ &= [A_{m,n}]\,[A_{m,s}]\,\{S_{m-1}\} = [A_m]\,\{S_{m-1}\}, \end{aligned} \tag{9}$$

where $[A_m]$ is the transfer matrix between nodes $m-1$ and m.

2.2 Influence of lintel beam on torsional rigidity of the core

The lintel beam is considered to be rectangular in cross section, where the end points are fixed to the core at points *a* and *b*, as seen in Fig. 3(b).

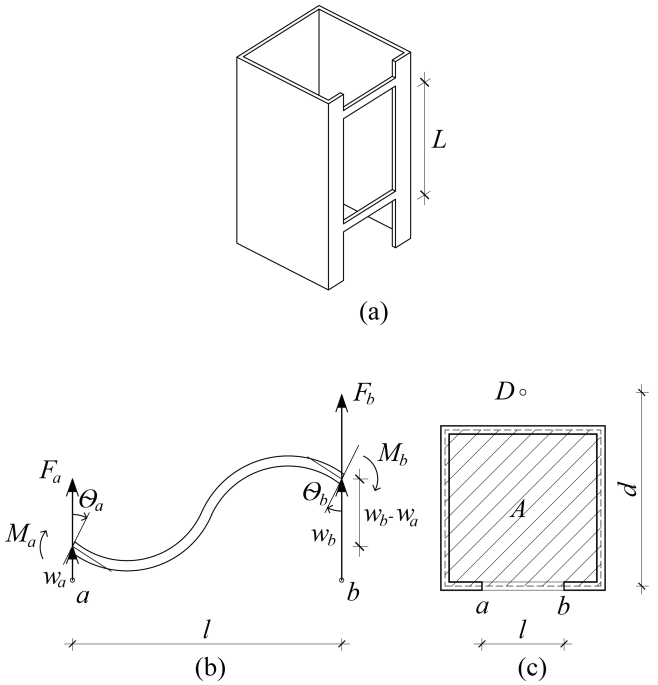

Fig. 3. Core with lintel beams (a); displacements and rotations of the end points of the beam at core warping (b); cross section of the core (c)

The effect of lintel beam is to restrain the longitudinal deformations (warping) of the core resulting from torsion. With respect to the adopted assumptions, during the bending of the core, around *X* or *Y* axes, cross sections do not deform and remain plane, so it does not affect the deformation of lintel beam.

The vertical displacements and rotations of the end points of the beam due to warping are:

$$\begin{aligned} w_a &= -\Omega_a \varphi', \\ w_b &= -\Omega_b \varphi', \\ \theta_a &= \theta_b = d\varphi', \end{aligned} \tag{10}$$

where Ω_a and Ω_b are the principal sectorial coordinates of the end points, d is the distance of the end points from the shear center. The beams are exposed to bending in the vertical plane only, causing reactive forces and moments in the endpoints:

$$\begin{aligned} F &= -F_a = F_b = \frac{12EI}{l^3(1+\alpha)}\left[w_b + w_a + \frac{l}{2}(\theta_a + \theta_b)\right], \\ M &= M_a + M_b = F\,l, \end{aligned} \tag{11}$$

where I is the second moment of the area of the cross section in relation to the horizontal axis, l is the beam span, α is the shear area coefficient. Substituting (10) into (11)-1 yields:

$$F = \frac{12EI}{l^3(1+\alpha)}(\Omega_a - \Omega_b + l\,d)\,\varphi' = \frac{12EI}{l^3(1+\alpha)}2A\varphi', \tag{12}$$

where A is the area enclosed by the cross section of the core, as shown in Fig. 3(c).

The influences of reactive forces and moments on torsional rigidity of the core may be accounted for by external bimoment [16]:

$$\bar{B}^b = F(\Omega_a - \Omega_b + ld) = F \cdot 2A. \tag{13}$$

Finally, substituting (12) into (13) yields bimoment in the node *m* of core, caused by the beam:

$$\bar{B}^b = \frac{48EI}{l^3(1+\alpha)}A^2\varphi' = R^b\varphi', \tag{14}$$

where R^b is the bimoment caused by beam for $\varphi' = 1$.

2.3 Influence of floor slab on torsional rigidity of the core

The floor slab in this study is treated as a plate of constant thickness which is simply supported by the core along the inner edge, while along the outer edge it is free of restraints (see Fig. 4). Subsequently, the influence of boundary conditions - i.e. the type of restraints along the outer edge of the floor slabs - on the NFs is checked by a comparative analysis, the details of which are provided in Section 3.

The application of the here presented, rather simplified boundary conditions is justified by the fact that influences in the floor slabs induced by vertical movements of the core are significantly decreased by the distance from the core. Similar to the lintel beams, floor slabs deform only by warping, while due to the bending of the core, the floor slabs rotate around *X* or *Y* axes without deformation, as rigid bodies.

The vertical displacement of any common point P_i of the core is:

$$w_i = -\varphi'\Omega_i. \tag{15}$$

The plate is exposed to displacements and rotation at these points, causing support reactions (axial forces and moments), which can be calculated using FEM.

Force F_i and moment M_i stemming from the known displacement pattern of the plate, represent external concentrated load of the core at point P_i. Their influence on the core can be taken as the external bimoment (according to [3]):

$$\bar{B}^{pl} = R^{pl}\varphi', \tag{16}$$

where

$$R^{pl} = \sum_{i=1}^{N_j} F_i\Omega_i + \sum_{i=1}^{N_j} M_i\frac{d}{ds}\Omega_i, \tag{17}$$

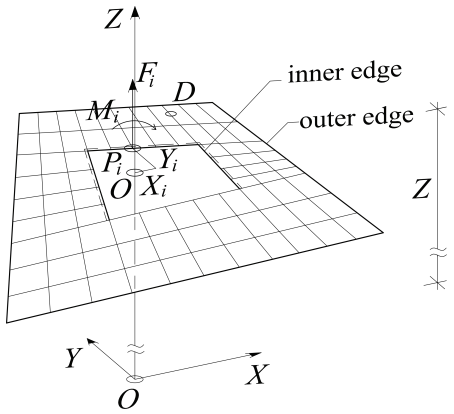

Fig. 4. Cross section of the core and the corresponding floor slab

is the external bimoment in the node due to unit warping, $\varphi' = 1$. N_j is the total number of calculation points P_i along the contact of the core and the slab.

The sum of the influence of the lintel beam (14) and floor slab (16) in the node of the thin-walled beam yields the total bimoment:

$$\bar{B} = \bar{B}^b + \bar{B}^{pl} = \left(R^b + R^{pl}\right)\varphi' = R\,\varphi'. \tag{18}$$

2.4 Calculation of NFs

Knowing the influence in node 0, the influence in the top node *n* of the thin-walled beam is determined by:

$$\{S_n\} = [A_n]\,[A_{n-1}]\ldots[A_1]\,\{S_0\} = \left[\bar{A}_n\right]\{S_0\}, \tag{19}$$

where $\left[\bar{A}_n\right]$ is the transfer matrix between the bottom node 0, and the top node, *n*, of the thin-walled beam.

The following are the boundary conditions at the bottom and top of the thin-walled beam, six at each end:

$$\begin{aligned} &U_0 = U_0' = V_0 = V_0' = \Phi_0 = \Phi_0' = 0, \\ &M_{Y,n} = Q_{X,n} = M_{X,n} = Q_{Y,n} = B_n = T_n = 0, \end{aligned} \tag{20}$$

installed into the state vectors in Eq. (19), yields a system of six homogenous algebraic equations, which has a nontrivial solution only if the system determinant equals zero, i.e.:

$$\det\left|\left[\bar{A}_n\left(\omega_j\right)\right]_H\right| = 0. \tag{21}$$

Solving (21) in respect to ω_j yields the system circular NFs.

2.5 Computer program for calculation of NFs of the model

Based on the method described above a computer program TWBEIG written in Visual Fortran was developed.

Program TWBEIG searches for the solution by sweeping through a given frequency range by a default frequency step. The process of computation is as follows:

- before starting the program TWBEIG, the external bimoment in the node due to unit warping R^{pl} needs to be determined by (17), using FEM.
- The stiffness of the constitutive elements is then calculated by the activated TWBEIG, based on geometry and the and properties of materials used;
- generates transfer matrices given by (9) and (19);
- calculates the value of the determinant in (21) at each frequency, until the change of its sign occurs.
- The frequency corresponding to the sign change represents one of the NFs in the given frequency range.
- The same procedure is repeated until all NFs are determined.

The accuracy of the solution is determined by the applied frequency step, which can be adopted arbitrarily.

3 Numerical examples

In order to illustrate the efficacy of the proposed numerical method, and to investigate the influence of lintel beams and floor slabs on NFs of the tall buildings core, two numerical cases will be used.

Example 1.

The first example is a simple, fifteen-storey single core tall building, used previously in papers [1], [3] and [4]. The dimensions are shown in Fig. 5 and Fig. 6.

The input parameters required by the program are as follows:

- parameters describing the material:

E $= 27.6 \cdot 10^6$ kN/m^2,
G $= 12.0 \cdot 10^6$ kN/m^2,
ρ $= 2.5492 \cdot 10^3$ kg/m^3;

- parameters describing the core:

I_{XX} $= 38.77$ m^4,
I_{YY} $= 30.51$ m^4,
$I_{\Omega\Omega}$ $= 300.0$ m^6,
K $= 0.190$ m^4;

- parameters describing the beam:

l $= 3.048$ m,
α $= 0.062$,
A $= 0.139$ m^2,
I $= 2.462 \cdot 10^{-3}$ m^4,
R^b $= 120.13 \cdot 10^9$ Nm^3,

- parameters describing the floor slabs are:

M $= 109322$ kg,
Y_{DC} $= 5.826$ m,
J_D $= 6.7064 \cdot 10^6$ kgm^2

in nodes 1-14, while

M $= 79528$ kg,
Y_{DC} $= 5.901$ m,
J_D $= 5.3837 \cdot 10^6$ kgm^2

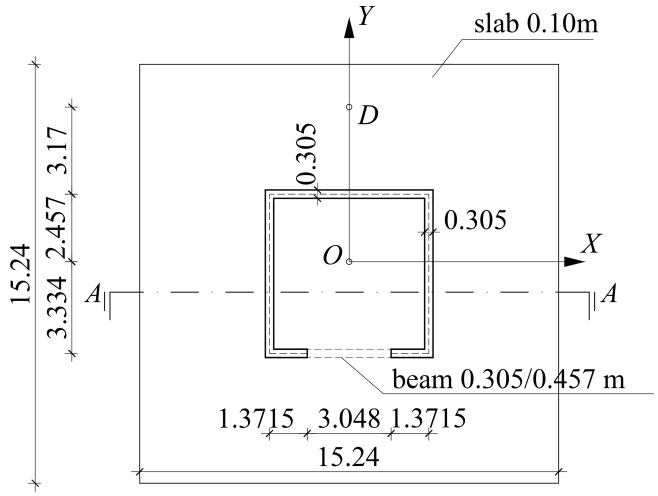

Fig. 5. Base plot of the numerical example

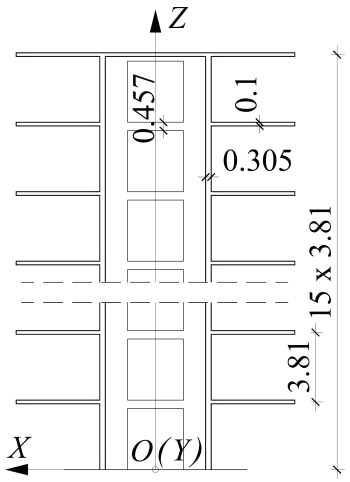

Fig. 6. Cross section of the numerical example

in node 15.

$X_{DC} = 0\,\text{m}$, and $R^{pl} = 3336.5 \cdot 10^6\,\text{Nm}^3$ for all nodes. R^{pl} is determined by (17) as described in Section 2.3.

In order to investigate the influence of lintel beams and floor slabs on the dynamic characteristics of the core, four cases of calculation have been considered:

- case TWB-1, the stiffness characteristics of the beams and floor slabs were both taken into account;
- case TWB-2, the stiffness characteristic of beams are taken into account only;
- case TWB-3, the stiffness characteristic of floor slabs are taken into account only;
- case TWB-4, the stiffness characteristics of both beams and floor slabs are neglected.

In all four cases the mass of the core and floor slabs are taken into account, while the mass of beams are neglected as minor, compared to the ones mentioned above.

For the FEM analysis, Four-node Quadrilateral Shell Elements are used: 90 elements in each storey for the floor slabs and 36 elements in each segment of the core. Each beam was modeled by 2 Frame Elements of Rectangular shape. The number of calculation points along the contact of the core and the slab is 13. The details of the applied boundary conditions are as follows:

- the joints of the core elements at the bottom level are fully restrained;
- joints on the outer edge of floor slabs are free of restrains;
- the vertical displacement of the slab and the core must be compatible in the joints.

The results both of the TWBEIG and FEM analyses, together with the relative differences, are presented in Table 1, Table 2, Table 3 and Table 4.

Tab. 1. NFs of the case TWB-1

Reference		FEM	TWBEIG	
j	mode	Freq. [Hz]	Freq. [Hz]	Diff. (%)
1^{st}	$X-\Phi$	0.65854	0.68325	-3.61
2^{nd}	Y	0.88688	0.89954	-1.41
3^{rd}	$X-\Phi$	1.82773	1.79320	1.93

Tab. 2. NFs of the case TWB-2

Reference		FEM	TWBEIG	
j	mode	Freq. [Hz]	Freq. [Hz]	Diff. (%)
1^{st}	$X-\Phi$	0.65372	0.67943	-3.78
2^{nd}	Y	0.88688	0.89954	-1.41
3^{rd}	$X-\Phi$	1.81109	1.78795	1.29

The values of NF show significant agreement between the FEM and TWBEIG results. The first and third mode correspond

Tab. 3. NFs of the case TWB-3

Reference		FEM	TWBEIG	
j	mode	Freq. [Hz]	Freq. [Hz]	Diff. (%)
1^{st}	$X-\Phi$	0.43660	0.44627	-2.17
2^{nd}	Y	0.88682	0.89954	-1.41
3^{rd}	$X-\Phi$	1.65902	1.62195	2.28

Tab. 4. NFs of the case TWB-4

Reference		FEM	TWBEIG	
j	mode	Freq. [Hz]	Freq. [Hz]	Diff. (%)
1^{st}	$X-\Phi$	0.41533	0.42399	-2.04
2^{nd}	Y	0.88682	0.89954	-1.41
3^{rd}	$X-\Phi$	1.64112	1.60619	2.17

to the flexural-torsional vibration mode, and the second is only the flexural mode in Y direction.

The comparison of the results TWB-1 with TWB-3 and TWB-2 with TWB-4 highlights the influence of lintel beams on NFs.

It is obvious that lintel beams have a significant influence on the first NF (approximately 55% in both cases), much less on the third (10%), while they do not affect the second NF at all. This was expected, since lintel beams do not deform in this mode.

Similarly, the influence of floor slabs on NFs can be seen by the comparison of results TWB-1 with TWB-2, and TWB-3 with TWB-4. The floor slabs evidently modify NF much less than lintel beams do (up to 5% only). No change in the second NF has been detected, for the same reason as in the case of the beams.

Fig. 7 shows the variation of the first and third mode of NFs of the core in function of the height of lintel beams (H), calculated by TWBEIG and FEM.

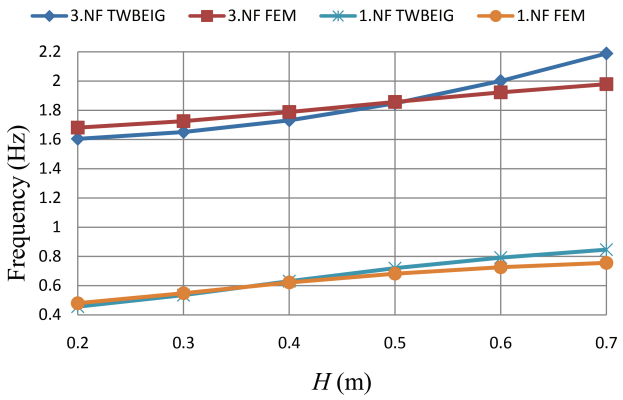

Fig. 7. Change of the first and third NF by varying beam height

Fig. 7 demonstrate minor differences in NFs between the TWBEIG and FEM results all through the analyzed range. The increase of the beam height produced a rising of the first and third NF.

A comparative analysis is performed, using FEM, in order to gain insight into the influence of the boundary condition along the outer edge of the slab on the NF. The boundary conditions considered are as follows:

- the outer edge is free of restraints, and
- the outer edge is simple supported.

This investigation is accomplished for the case TWB-1. The results are summarized in Table 5.

Tab. 5. Comparative analysis of boundary conditions along the outer edge of floor slabs, case the TWB-1

Reference		Free of restraint	Simply supported	
j	mode	Freq. [Hz]	Freq. [Hz]	Diff. (%)
1^{st}	$X-\Phi$	0.65854	0.66293	0.67
2^{nd}	Y	0.88688	0.89567	0.99
3^{rd}	$X-\Phi$	1.82773	1.83368	0.33

It is evident that in the analyzed case the considered boundary conditions along the outer edge of floor slabs have no significant influence on the calculation results.

Example 2.

In this numerical example the results of experimental studies performed on a 15-storey plexiglass model of a tall building are compared with the results obtained by numerical methods.

Taking into account that floor slabs serve to hold the cross section in shape, thus satisfying a basic assumption for the Vlasov theory, the experimental results will be compare with TWBEIG and FEM results only for models with floor slabs.

Experimental models with and without lintel beams are denoted by PLX-1 and PLX-2, respectively. The height of a single storey is 77 mm. Plates of plexiglass XT, 2 and 6 mm thick were used in the model (Fig. 8). At the bottom, the model was glued to a plexiglass board $2 \cdot 10$ mm thick, which was fastened to a concrete floor.

The input parameters for TWBEIG program are:

- parameters describing the material:

$E \quad = 3000\ \mathrm{N/mm^2}$,
$G \quad = 1095\ \mathrm{N/mm^2}$,
$\rho \quad = 1190 \cdot 10^{-9}\ \mathrm{kg/mm^3}$;

- parameters describing the core:

$I_{XX} \quad = 3822.6 \cdot 10^3\ \mathrm{mm^4}$,
$I_{YY} \quad = 4934.7 \cdot 10^3\ \mathrm{mm^4}$,
$I_{\Omega\Omega} \quad = 12.628 \cdot 10^9\ \mathrm{mm^6}$,
$K \quad = 26784\ \mathrm{mm^4}$;

- parameters describing the beam:

$l \quad = 60\ \mathrm{mm}$,
$\alpha \quad = 0.074$,
$I \quad = 364.5\ \mathrm{mm^4}$,
$A \quad = 11664\ \mathrm{mm^2}$,
$R^b \quad = 30.782 \cdot 10^9\ \mathrm{Nmm^3}$,

- parameters describing floor slabs are:

$M \quad = 0.3878\ \mathrm{kg}$,
$Y_{DC} \quad = 107.9\ \mathrm{mm}$,

J_D $= 8.576 \cdot 10^6$ kgmm^2

in nodes 1-14, while

M $= 0.2855$ kg,
Y_{DC} $= 109.4$ mm,
J_D $= 7.019 \cdot 10^6$ kgmm^2

in node 15.

Parameters $R^{pl} = 1.1805 \cdot 10^9$ Nmm^3, $X_{DC} = 0$ mm are identical in all nodes.

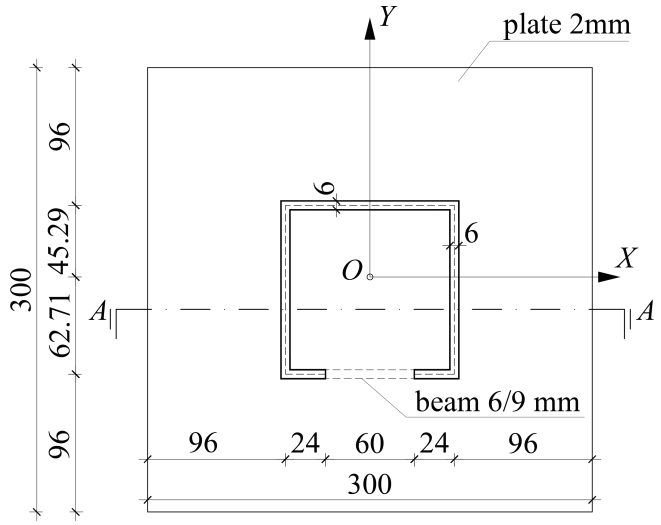

Fig. 8. Base plot of the experimental model PLX-1

Young modulus E was obtained by measurements, performed in the laboratories of the Faculty of Civil Engineering, Subotica, Serbia. The mass of the lintel beams and the mass of the accelerometers (together with the corresponding screws and connectors) fixed to the top node of the model were accounted for to make the calculations as close as possible to the experimental (physical) model.

In order to measure the dynamic response of the model, two IMI ICP Accelerometers (model 603C01) have been used. One of them was a control device. The signal was acquired and processed with VB2000™FFT Vibration Analyzer. The tested frequency range is 0 - 100 Hz, with a resolution of 800 lines, i.e. the frequency interval is 0.125 Hz. The analyzer has a built-in Bump Test function [17], which represents a simple method for analyzing the structural modal response of a machine or structure. It requires the hitting (bumping) of the structure with a hammer. During the measurements waveform records have been taken four times, which were immediately transformed into frequency spectrum by the analyzer. The resulting frequency spectrum was obtained by applying peak hold averaging, which is stored in the memory by the instrument. Further analysis of the recorded data was carried out by computer using ASCENT 2007+ software [18].

Points A-1 and A-2 of the cross section at the top of the model were chosen for the location of accelerometers, which preserved the symmetry of the model. The spots and direction of the hammer blows to the model are shown in Fig. 9. B-1 excites the first and third mode, which creates coupled flexural-torsional vibrations. B-2 excites vibrations in the direction of Y axis, which correspond to the second mode.

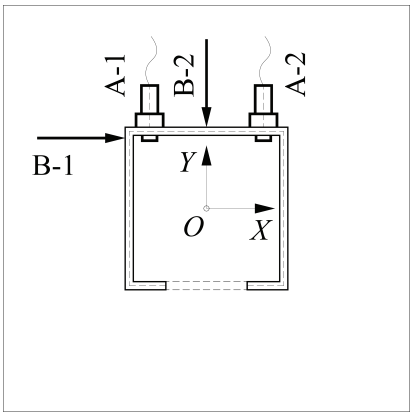

Fig. 9. Position of accelerometers and the direction of excitation

NFs of the experimental model PLX-1 correspond to the peaking frequencies in Fig. 10 and Fig. 11. The peaks and the corresponding frequencies are easily determined by ASCENT 2007+ software.

The outlined method to determining NFs is accurate enough for this type of model. Even though the study of the mode shape is beyond the scope of this paper, the combination of experimental tests and numeric results presented later in the paper, enable the identification of the mode shape and the corresponding NFs (according to Ambrosini [19] and [20]).

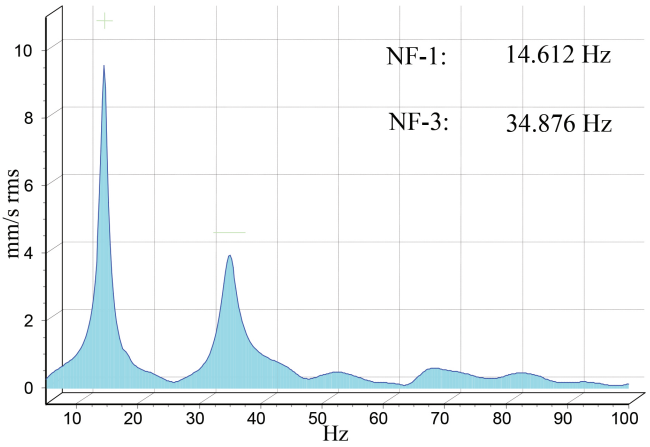

Fig. 10. Resulting frequency spectrum obtained by the experimental model PLX-1 (first and third mode)

In Table 6 and Table 7 the experimental values of NFs are compared with TWBEIG and FEM results.

The values of frequencies show reasonable agreement between the experimental and calculated TWBEIG and FEM results. Regarding the influence of lintel beams on the value of NF of the core, the same conclusions apply, as in the previous example.

4 Conclusions

The influence of lintel beams and floor slabs on NFs of tall buildings, braced by core walls was examined. For that pur-

Tab. 6. NFs of the model PLX-1

Reference		TEST	TWBEIG		FEM	
j	mode	Freq. [Hz]	Freq. [Hz]	Diff. (%)	Freq. [Hz]	Diff. (%)
1^{st}	$X-\Phi$	14.61	14.98	2.55	15.22	4.14
2^{nd}	Y	16.88	17.32	2.59	18.00	6.62
3^{rd}	$X-\Phi$	34.88	36.81	5.53	33.10	-5.09

Tab. 7. NFs of the model PLX-2

Reference		TEST	TWBEIG		FEM	
j	mode	Freq. [Hz]	Freq. [Hz]	Diff. (%)	Freq. [Hz]	Diff. (%)
1^{st}	$X-\Phi$	8.41	8.52	1.38	8.65	2.86
2^{nd}	Y	17.13	17.62	2.85	18.05	5.37
3^{rd}	$X-\Phi$	29.63	30.81	4.00	29.06	-1.45

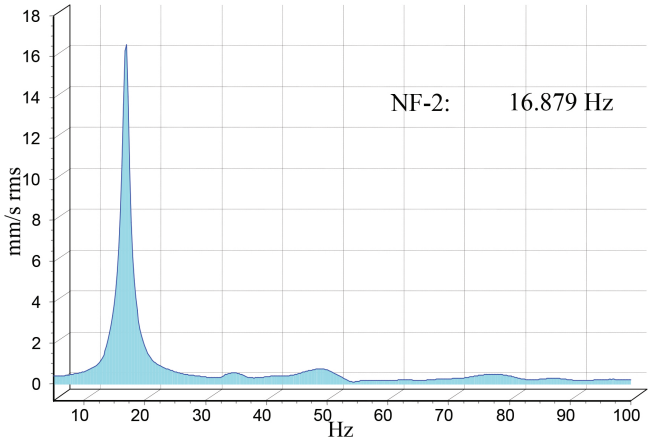

Fig. 11. Resulting frequency spectrum obtained by the experimental model PLX-1 (second mode)

pose a numerical procedure, based on the Vlasov theory of thin-walled beams and transfer matrix method, has been developed. The obtained results were compared with FEM and experimental results. Good agreement has been achieved.

Based on the analysis accomplished by the proposed method, the following can be concluded:

- Lintel beams have a significant effect on the NFs,
- while the effect of floor slabs is much lower.
- Boundary conditions along the outer edge of floor slabs have no significant influence on the calculated NFs.
- The proposed numerical method offers a solid base for creation of a simple computer model, suitable for the determination of NFs of the tall buildings core. The limited number of unknowns in the proposed model provides good control, easy and quick presentation and overview of the obtained results. It is simple and accurate enough to be used either for preliminary design or for final analysis.

The outlined method is suitable for the calculation of NFs of tall building braced by a single core, in the cases when the characteristics of the building meet the assumptions adopted in the proposed method sufficiently. The application of the proposed method is limited to cases where the foundation is stiff enough to comply with the related assumption declared in the Introduction, i.e. to provide near full restraint.

It is obvious that neglecting the shear deformation of the core introduces certain error in the results, however, it is not expected to have a significant influence on the impact of lintel beams and floor slabs - determined mostly by their geometry - on the NFs of tall buildings core.

Appendix

The transfer matrix of segment m:

$$[A_{m,s}] = \begin{bmatrix} 1 & L_m & \frac{L_m^2}{2} & -\frac{L_m^3}{6} & 0 & 0 & 0 & 0 & 0 & 0 & 0 & 0 \\ 0 & 1 & L_m & -\frac{L_m^2}{2} & 0 & 0 & 0 & 0 & 0 & 0 & 0 & 0 \\ 0 & 0 & 1 & -L_m & 0 & 0 & 0 & 0 & 0 & 0 & 0 & 0 \\ 0 & 0 & 0 & 1 & 0 & 0 & 0 & 0 & 0 & 0 & 0 & 0 \\ 0 & 0 & 0 & 0 & 1 & -L_m & -\frac{L_m^2}{2} & -\frac{L_m^3}{6} & 0 & 0 & 0 & 0 \\ 0 & 0 & 0 & 0 & 0 & 1 & L_m & \frac{L_m^2}{2} & 0 & 0 & 0 & 0 \\ 0 & 0 & 0 & 0 & 0 & 0 & 1 & L_m & 0 & 0 & 0 & 0 \\ 0 & 0 & 0 & 0 & 0 & 0 & 0 & 1 & 0 & 0 & 0 & 0 \\ 0 & 0 & 0 & 0 & 0 & 0 & 0 & 0 & 1 & \frac{\sinh\lambda_m}{k_m} & 1-\cosh\lambda_m & \frac{\lambda_m-\sinh\lambda_m}{k_m} \\ 0 & 0 & 0 & 0 & 0 & 0 & 0 & 0 & 0 & \cosh\lambda_m & -k_m\sinh\lambda_m & 1-\cosh\lambda_m \\ 0 & 0 & 0 & 0 & 0 & 0 & 0 & 0 & 0 & -\frac{\sinh\lambda_m}{k_m} & \cosh\lambda_m & \frac{\sinh\lambda_m}{k_m} \\ 0 & 0 & 0 & 0 & 0 & 0 & 0 & 0 & 0 & 0 & 0 & 1 \end{bmatrix},$$

where $k_m = \sqrt{\frac{GK_m}{EI_{\Omega\Omega,m}}}$ and $\lambda_m = k_m L_m$ are characteristic parameters of segment m.

The transfer matrix of node m:

$$[A_{m,n}] = \begin{bmatrix} 1 & 0 & 0 & 0 & 0 & 0 & 0 & 0 & 0 & 0 & 0 & 0 \\ 0 & 1 & 0 & 0 & 0 & 0 & 0 & 0 & 0 & 0 & 0 & 0 \\ 0 & 0 & 1 & 0 & 0 & 0 & 0 & 0 & 0 & 0 & 0 & 0 \\ \frac{-\omega^2 M_m}{EI_{XX,m}} & 0 & 0 & 1 & 0 & 0 & 0 & 0 & \frac{-\omega^2 M_m Y_{DC,m}}{EI_{XX,m}} & 0 & 0 & 0 \\ 0 & 0 & 0 & 0 & 1 & 0 & 0 & 0 & 0 & 0 & 0 & 0 \\ 0 & 0 & 0 & 0 & 0 & 1 & 0 & 0 & 0 & 0 & 0 & 0 \\ 0 & 0 & 0 & 0 & 0 & 0 & 1 & 0 & 0 & 0 & 0 & 0 \\ 0 & 0 & 0 & 0 & \frac{-\omega^2 M_m}{EI_{YY,m}} & 0 & 0 & 1 & \frac{\omega^2 M_m X_{DC,m}}{EI_{YY,m}} & 0 & 0 & 0 \\ 0 & 0 & 0 & 0 & 0 & 0 & 0 & 0 & 1 & 0 & 0 & 0 \\ 0 & 0 & 0 & 0 & 0 & 0 & 0 & 0 & 0 & 1 & 0 & 0 \\ 0 & 0 & 0 & 0 & 0 & 0 & 0 & 0 & 0 & \frac{-R_m}{GK_m} & 1 & 0 \\ \frac{-\omega^2 M_m Y_{DC,m}}{GK_m} & 0 & 0 & 0 & \frac{\omega^2 M_m X_{DC,m}}{GK_m} & 0 & 0 & 0 & \frac{-\omega^2 J_{D,m}}{GK_m} & 0 & 0 & 1 \end{bmatrix},$$

Acknowledgement

The project presented in this article is supported by The Ministry of Education and Science of the Republic of Serbia (Project No. ON174027).

References

1 **Liauw TC, Luk WK**, *Torsion of core walls of nonuniform section*, Journal of the Structural division, **106**(9), (1980), 1921–1931.

2 **Mendis P**, *Warping analysis of concrete cores*, The Structural Design of Tall Buildings, **10**(1), (2001), 43–52, DOI 10.1002/tal.160.

3 **Smith BS, Taranath BS**, *The analysis of tall core-supported structures subject to torsion*, Proceedings of the Institution of Civil Engineers, **53**(2), (1972), 173–187, DOI 10.1680/iicep.1972.5408.

4 **Heidebrecht AC, Smith BS**, *Approximate analysis of open-section shear walls subject to torsional loading*, Journal of the Structural Division, **99**(12), (1973), 2355–2373.

5 **Ng SC, Kuang JS**, *Coupled vibration of structural thin-walled cores*, Acta Mechanica Solida Sinica, **13**(1), (2000), 81–88.

6 **Kuang JS, Ng SC**, *Coupled vibration of tall building structures*, The Structural Design of Tall and Special Buildings, **13**(4), (2004), 291–303, DOI 10.1002/tal.253.

7 **Mehtaf SA, Tounsi A**, *Vibration characteristics of tall buildings braced by shear walls and thin-walled open-section structures*, The Structural Design of Tall and Special Buildings, **17**(1), (2008), 203–216, DOI 10.1002/tal.346.

8 **Rafezy B, Howson WP**, *Coupled lateral-torsional frequencies of asymmetric, three-dimensional structures comprising shear-wall and core assemblies with stepwise variable cross-section*, Engineering Structures, **31**(8), (2009), 1903–1915, DOI 10.1016/j.engstruct.2009.01.024.

9 **Kheyroddin A, Abdollahzadeh D, Mastali M**, *Improvement of open and semi-open core wall system in tall buildings by closing of the core section in the last story*, International Journal of Advanced Structural Engineering (IJASE), **6**(3), (2014), 1–12, DOI 10.1007/s40091-014-0067-0.

10 **Zalka KA**, *Maximum deflection of symmetric wall-frame buildings*, Periodica Polytechnica Civil Engineering, **57**(2), (2013), 173–184, DOI 10.3311/PPci.7172.

11 **Zalka KA**, *Maximum deflection of asymmetric wall-frame buildings under horizontal load*, Periodica Polytechnica Civil Engineering, **58**(4), (2014), 387–396, DOI 10.3311/PPci.7084.

12 **Kollár PL**, *Flexural–torsional vibration of open section composite beams with shear deformation*, International Journal of Solids and Structures, **38**(42-43), (2001), 7543–7558, DOI 10.1016/S0020-7683(01)00025-7.

13 **Pluzsik A, Kollár PL**, *Effects of Shear Deformation and Restrained Warping on the Displacements of Composite Beams*, Journal of Reinforced Plastics and Composites, **21**(17), (2002), 1517–1541, DOI 10.1177/0731684402021017927.

14 **Potzta G, Kollár PL**, *Analysis of building structures by replacement sandwich beams*, International Journal of Solids and Structures, **40**(3), (2003), 535–553, DOI 10.1016/S0020-7683(02)00622-4.

15 **Zalka KA**, *A simple method for the deflection analysis of tall wall-frame building structures under horizontal load*, The Structural Design of Tall and Special Buildings, **18**(3), (2009), 291–311, DOI 10.1002/tal.410.

16 **Prokić A**, *Effect of Bracing on Linear Free Vibration Characteristics of Thin-Walled Beams with Open Cross Section*, Journal of Engineering Mechanics, **136**(3), (2010), 282–289, DOI 10.1061/(ASCE)0733-9399(2010)136:3(282).

17 *VB 2000 Instrument reference guide*, Commtest Instruments Ltd; Christchurch, New Zealand, 2006.

18 *Ascent software reference guide*, Commtest Instruments Ltd; Christchurch, New Zealand, 2007.

19 **Ambrosini D**, *On free vibration of nonsymmetrical thin-walled beams*, Thin-Walled Structures, **47**(6-7), (2009), 629–636, DOI 10.1016/j.tws.2008.11.003.

20 **Ambrosini D**, *Experimental validation of free vibrations from nonsymmetrical thin walled beams*, Engineering Structures, **32**(5), (2010), 1324–3332, DOI 10.1016/j.engstruct.2010.01.010.